InAs-Based Mid-Infrared Interband Cascade Lasers Near 5.3 μm

Zhaobing Tian, *Member, IEEE*, Yuchao Jiang, Lu Li, Robert T. Hinkey, Zuowei Yin, Rui Q. Yang, *Senior Member, IEEE*, Tetsuya D. Mishima, Michael B. Santos, and Matthew B. Johnson

***Abstract*— InAs-based interband cascade (IC) lasers with dielectric-metal hybrid top cladding layers were demonstrated at emission wavelengths near 5.3 μm for temperatures up to 248 K in continuous wave mode and 300 K in pulsed mode. Preliminary experimental results showed that these hybrid waveguide IC lasers had slightly better device performances in terms of operating temperature, compared to IC lasers with InAs plasmon cladding layers on both sides. The threshold current densities of these IC lasers were as low as 12 A/cm^2 with voltage efficiency above 96% at 80 K. The output power of these IC lasers reached 120 mW/facet and a power efficiency of 21% was obtained at 80 K.**

***Index Terms*— Diode lasers, mid-infrared, optical waveguide.**

I. Introduction

BECAUSE of their low threshold current, interband cascade (IC) lasers [1] are emerging as efficient mid-infrared (IR) laser sources for low-threshold power consumption applications (*e.g.*<0.1 W) in continuous wave (cw) operation at room temperature [2–6]. By employing plasmon-waveguide structures [7–10], the spectral coverage of IC lasers can be further extended to the long-wavelength IR region [11]. In these long-wavelength IC lasers, the cladding layer becomes thicker and the waveguide loss may increase significantly, presenting challenges for the material growth and difficulty in achieving high device performance. Hence, it is desirable and important to find ways to reduce the cladding layer thickness and suppress the waveguide loss.

Considering that long-wavelength IC lasers typically utilize ridge widths wider than 10 μm to minimize the surface recombination, the dielectric layer (usually made of SiO_2 or Si_3N_4) underneath the metal bonding pad can cover the majority of the laser ridge, while the metal contact to the ridge can be made to be only 2-3 μm. Here we show that this dielectric layer, which is conventionally used for insulation and passivation of ridge waveguide lasers, also has properties that make it a favorable choice to form the top cladding layer of the laser waveguide. Typically, these materials have weak absorption in the mid-IR, and their large refractive index contrast with the active region (1.4 for SiO_2 versus ~3.47 for the active region) enables good mode confinement. Although the top metal layer directly on the ridge can introduce some optical loss, it is minimized with a narrow contact (2-3 μm). Moreover, optical loss associated with mode leakage into the metal contact is significantly less in IC lasers, based on transverse electric (TE) modes, as compared to that in quantum cascade (QC) lasers, based on transverse magnetic (TM) modes. TE modes (unlike TM modes [12]) are not coupled to lossy surface plasmon modes, and certain metals are actually suitable choices as cladding materials in the mid-IR. The insertion of a thin dielectric layer (with a small refractive index and low absorption losses), between semiconductor and metal layers, will decrease the optical field intensity that penetrates into the high loss metal cladding layers, thereby suppressing the optical waveguide loss. Thus, with a properly designed dielectric-metal hybrid top cladding layers, the top semiconductor-plasmon cladding layer may not be necessary in IC lasers. In addition to the optical favorability of this approach, there are also several practical advantages such as simplified material growth and the ease to integrate distributed feedback gratings on top of the ridge.

In this paper, we present our recent implementation and investigation of dielectric and metal layers as the top cladding layers for IC lasers with emission wavelengths near 5.3 μm. We compare this approach with the alternative approach of using an InAs plasmon top cladding layer. Both the theoretical and experimental results show that IC lasers with the top dielectric-metal waveguide cladding have operating characteristics slightly better than IC lasers with the top semiconductor plasmon cladding layer. The IC lasers with

Manuscript received December 22, 2011; revised April 4, 2012; accepted April 7, 2012. Date of publication April 26, 2012; date of current version May 8, 2012. This work was supported in part by National Science Foundation under Grant ECCS-1002202 and C-SPIN, Oklahoma/Arkansas MRSEC under Grant DMR-050550, and the Center for Integrated Nanotechnologies, U.S. Department of Energy, Office of Basic Energy Sciences user facility at Sandia National Laboratories under Contract DE-AC04-94AL85000.

Z. Tian, Y. Jiang, L. Li, and R. Q. Yang are with the School of Electrical and Computer Engineering, University of Oklahoma, Norman, OK 73019 USA (e-mail: zbtian@ou.edu; yuchao.jiang@ou.edu; lilu@ou.edu; rui.q.yang@ou.edu).

R. T. Hinkey is with the School of Electrical and Computer Engineering, University of Oklahoma, Norman, OK 73019 USA, and also with the Homer L. Dodge Department of Physics and Astronomy, University of Oklahoma, Norman, OK 73019 USA (e-mail: robert.t.hinkey-1@ou.edu).

Z. Yin is with the School of Electrical and Computer Engineering, University of Oklahoma, Norman, OK 73019 USA, and also with the Nanjing National Laboratory of Microstructures and School of Engineering and Applied Sciences, Nanjing University, Nanjing 210093, China (e-mail: yinzuowei@gmail.com).

T. D. Mishima, M. B. Santos, and M. B. Johnson are with the Homer L. Dodge Department of Physics and Astronomy, University of Oklahoma, Norman, OK 73019 USA (e-mail: mishima@ou.edu; santos@nhn.ou.edu; matthew.b.johnson-2@ou.edu).

Color versions of one or more of the figures in this paper are available online at http://ieeexplore.ieee.org.

Digital Object Identifier 10.1109/JQE.2012.2195477

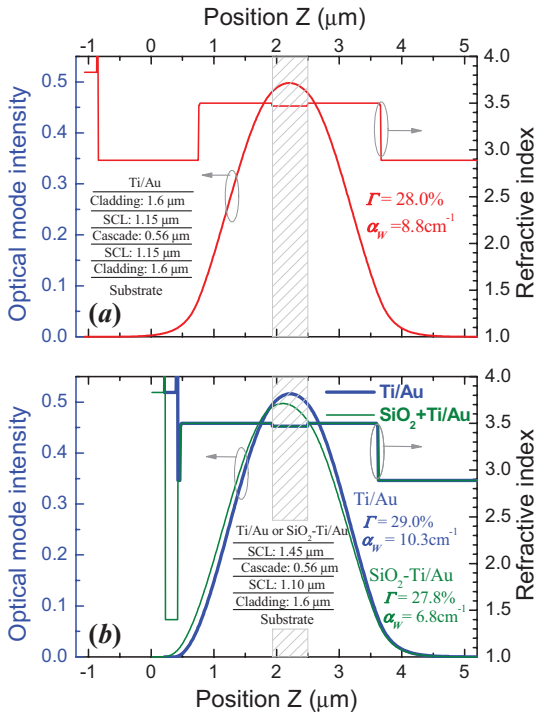

Fig. 1. Optical mode and refractive index profile along the growth direction of the InAs-based IC lasers (a) with the top InAs plasmon cladding layer and (b) without the top InAs plasmon cladding layers. The blue (thick) line corresponds to an IC laser directly using metal (Ti/Au) as the top cladding layer; the green (thin) line indicates an IC laser with a 200-nm-thick SiO_2, 20-nm-thick Ti, and a 220-nm-thick Au layer as the top cladding layers. The inserts show schematics of their waveguide structures.

the hybrid dielectric-metal top cladding operated in pulsed mode up to 300 K with emission wavelength near 5.3 μm.

II. Optical Waveguide and Device Structures

A one-dimensional (1D) waveguide model based on the transfer matrix method and a two-dimensional (2D) model using effective index method, were adopted to make a theoretical comparison of the different waveguide configurations. The optical constants of metals are from Ref. 13, and the dielectric constants for both nominally undoped and highly doped InAs were estimated from the Drude-Lorentz model using a theoretically evaluated doping-dependent effective mass [14] and an empirical model for the doping-dependent mobility [15]. In the calculation, optical absorption losses due to intersubband transitions and excess non-equilibrium carriers in the cascade region are not included. Our conclusions should not be influenced by this, because the optimal mode profile is only weakly dependent on the absorption coefficient of the active region.

Two InAs-based IC laser structures (wafers A and B) with different top waveguide configurations were first studied. The waveguide core for wafer A (B) is composed of the cascade region sandwiched between a 1.15-μm-thick (1.10-μm-thick) nominally undoped InAs bottom separate confinement layer (SCL) and a 1.15-μm-thick (1.45-μm-thick) undoped InAs top SCL. A 1.6-μm-thick n^{++}-type InAs (Si doped to 1×10^{19} cm^{-3}) plasmon layer was used as the bottom cladding

TABLE I
Calculated Optical Confinement Factor and Waveguide Loss of IC Lasers at a Wavelength of 5.3 μm at 300 K

Wafer	Top cladding configurations	Confinement factor (%)	Waveguide loss (cm^{-1})
A: InAs top plasmon layer	Ti/Au	28.0	8.8
	SiO_2-Ti/Au	28.0	8.8
B: no InAs top plasmon layer	Ag	29.2	7.6
	Au	29.1	8.1
	Ti/Au	29.0	10.3
	SiO_2-Au	27.9	5.9
	SiO_2-Ag	27.9	5.7
	SiO_2-Ti/Au	27.8	6.8

layer for both IC laser configurations. A slightly thicker top SCL in wafer B is used to reduce possible free-carrier loss introduced by the metal strips directly in contact with the top ridge. The two IC laser structures have a nominally identical 10-stage interband cascade region (total thickness 0.56 μm). The refractive index of the cascade region was estimated to be 3.47 at 5.3 μm and 300 K. Wafer A used a 1.6-μm-thick n^{++}-type InAs plasmon layer as the top waveguide cladding; and wafer B, with only a very thin (35 nm) n^{++}-type InAs contact layer, used a dielectric (SiO_2) and a metal (Ti/Au) layer as the top waveguide cladding.

Figure 1 presents a series of 1D optical mode profiles for different IC laser waveguide configurations. Figure 1(a) shows the optical mode and refractive index profile of wafer A, which uses the conventional n^{++}-InAs plasmon layer for both top and bottom cladding. For this configuration, the estimated confinement factor (Γ) and waveguide loss (α_w) were 28.0% and 8.8 cm^{-1}, respectively. Figure 1(b) shows the theoretical results for wafer B under the assumption that the top cladding layer is composed of: (1) only Ti/Au and (2) a thin layer (200 nm) of SiO_2 followed by Ti/Au. The confinement factors and waveguide losses for configurations (1) and (2) are 29.0% and 27.8%, respectively and 10.3 cm^{-1} and 6.8 cm^{-1}, respectively. The high loss for the purely metal-clad waveguide configuration is largely due to the poor optical properties of titanium, which, despite being very thin, introduces a significant amount of loss. However, in the hybrid dielectric-metal waveguide this loss is minimized by the insertion of a low loss dielectric layer and the use of narrow metal contacts for current injection. Based on our theoretical estimates of the waveguide loss and confinement factor, we find that this hybrid dielectric-metal waveguide approach should yield a device performance comparable or superior to the InAs-plasmon waveguide, by reducing the minimal gain required to reach threshold.

In future work, we plan to fabricate structures that alleviate the excessive loss introduced by Ti by introducing alternative materials. In Table 1, we present the predicted effects of inserting a layer of silver or gold between the semiconductor and the Ti/Au contact. As shown, we estimate this approach can reduce the waveguide loss by ~1.2 cm^{-1} at 5.3 μm.

R48

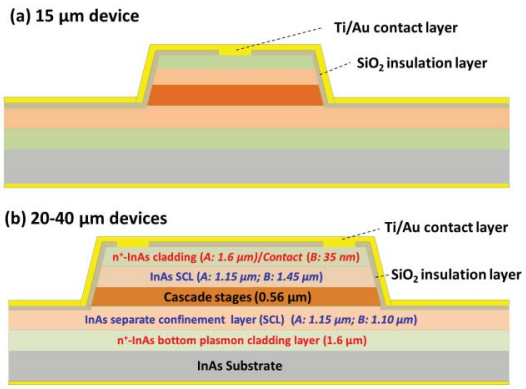

Fig. 2. Schematic cross section of the ridge waveguide IC lasers with different top cladding and contact configurations. (a) IC lasers with ridge width of 15 μm. (b) IC laser with ridge width of 20, 30, and 40 μm. The 3-μm-wide metal contact strips for the 15-μm-wide IC lasers lie in the center of the ridge, and the two contact strips are about 2 μm away from each edge for 20-, 30-, 40-μm-wide ridges.

The laser structures were grown using a Gen-II molecular beam epitaxy (MBE) system, equipped with group V crackers, on n^+-doped (100) InAs substrates. The active region of the cascade stages consists of AlSb/InAs/GaInSb/InAs/AlSb coupled quantum wells (QWs) sandwiched between the electron and hole injectors [4], which are composed of InAs/AlSb and GaSb/AlSb QWs, respectively. The active region, along with the electron and hole injectors together form one cascade stage. Compared to previous plasmon-waveguide IC lasers [9–10], the electron injector is shorter [4, 16] with the first InAs QW width 6.1 nm, and the hole injector is enhanced with two QWs [4], for suppressing possible leakage current. The entire cascade-stage region is designed with AlAs and GaAs interfaces to achieve strain balance and enhance carrier confinement. It should be noted that the *n*-doping in the electron injector is low ($\sim 1.5\times10^{17}$ cm^{-3}) for these IC lasers in contrast to the high *n*-doping recently reported for carrier rebalance in GaSb-based IC lasers [5, 6].

After growth, the wafers were processed into ridge waveguide lasers, with ridge widths between 15 and 40 μm, by using contact photolithography and wet etching. A 200-nm SiO_2 dielectric layer was deposited, narrow strips were opened for electrical contact on the top of the ridges (see Fig. 2.), and Ti(20nm)/Au(220nm) metal contact layers were then deposited on the top and bottom of the thinned wafers. As noted above, the SiO_2 and Ti/Au layers also served as the top waveguide cladding layers for devices made from wafer B. As shown in Fig. 2, there are two 3-μm-wide top metal contact strips near both edges, for the 20, 30, and 40-μm-wide ridges (similar to distributed feedback IC lasers [17]), and one top metal contact strip at the center for the 15-μm-wide ridge. These contacts are kept narrow in order to minimize the optical loss due to absorption in the metals, and ensure that the overall waveguide loss is close to the 1D value found for the hybrid dielectric-metal waveguide. To validate this, simulations for the 2D waveguides shown in Fig. 2 were carried out using the effective refractive index method. The 2D waveguide simulations found that the confinement

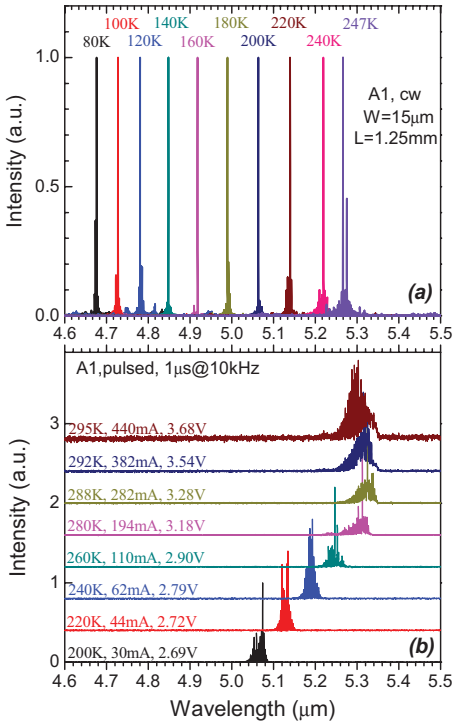

Fig. 3. Measured lasing spectra of a 15-μm-wide and 1.25-mm-long IC laser (denoted as A1) from wafer A operating in both (a) cw and (b) pulsed modes at different heat sink temperatures. The pulsed lasing spectra were shifted vertically for clarity.

factor is essentially same for wafer A and wafer B, while the waveguide optical loss is lower for all ridge widths in wafer B (*e.g.*, 7.4 cm^{-1} for 20-μm-wide ridge and 6.9 cm^{-1} for 30-μm-wide ridge) than in wafer A (8.8 cm^{-1}), consistent with expectations. However, the 15-μm-wide ridge laser from wafer B with the center metal contact would lase first on the first-excited lateral mode with a waveguide loss (7.0 cm^{-1}) that is lower than the waveguide loss (8.0 cm^{-1}) of the fundamental lateral mode. This results in a divergent double-lobe optical beam (also present in our earlier IC lasers [18]), making it difficult to effectively collect the optical output power from 15-μm narrow-ridge devices. Therefore optical output power measurements are only presented for 20- or 30-μm-wide laser devices.

The processed wafers were cleaved into laser bars with cavity lengths of 1-3 mm with both facets left uncoated, and then mounted epi-side-up on copper heatsinks for measurements. The optical power of the fabricated lasers was measured by a thermopile power meter for cw operation, and by a calibrated liquid-nitrogen cooled mercury-cadmium-telluride (MCT) detector in pulsed mode. A Nicolet Fourier transform infrared spectrometer was used to acquire the lasing spectra.

III. Experimental Results

R49

Devices made from wafer A (n^{++}-InAs plasmon top cladding) are able to operate in both cw and pulsed modes at temperatures well above 220 K. Fig. 3 shows cw and pulsed lasing spectra from a 15-μm-wide and 1.25-mm long device (denoted as A1) that lased at temperatures up to 247 K near

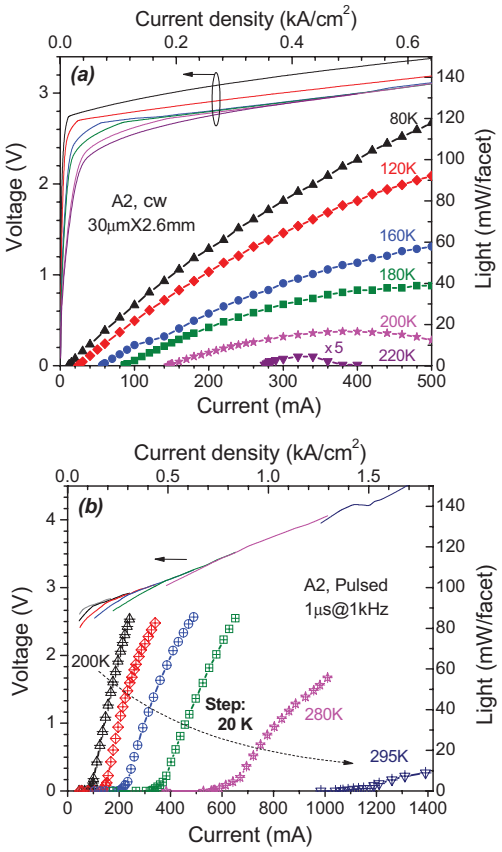

Fig. 4. Measured *I–V–L* characteristics of a 30-μm-wide and 2.6-mm-long IC laser (A2) from wafer A operating in both (a) cw and (b) pulsed modes at different heat sink temperatures.

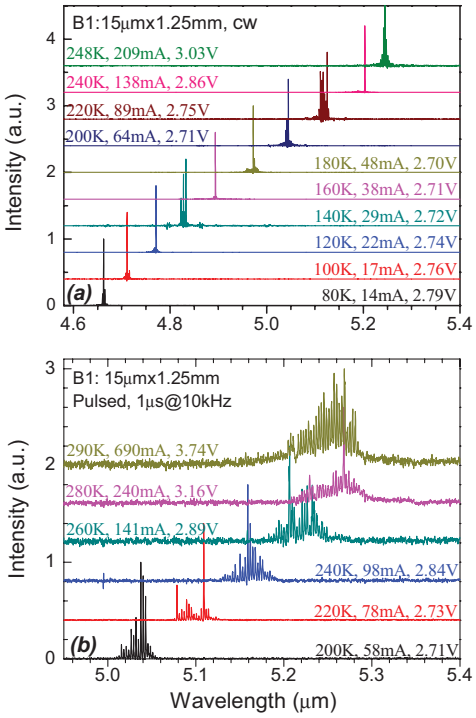

Fig. 5. Normalized lasing spectra of a 15-μm-wide and 1.25-mm-long laser (B1) made from wafer B operating in both (a) cw and (b) pulsed mode (1-μs pulse at 10 kHz) at different heat sink temperatures. The intensity of the lasing spectra is vertically shifted for clarity.

5.27 μm in cw mode (a), and up to 295 K near 5.3 μm in pulsed mode (b). The maximum cw operating temperature of 247 K is higher than the 229 and 165 K reported for earlier IC lasers with superlattice (SL) cladding layers and similar low n-doped electron injectors at the comparable wavelengths of 5.1 and 5.4 μm, respectively [19, 20]. These earlier devices with SL cladding layers lased in pulsed mode at temperatures up to 295 K near 5.24 μm [19] and 260 K near 5.7 μm [20], which are significantly higher than their maximum cw operating temperatures. This result corroborates our earlier suggestion [9] ~~that plasmon-waveguide IC lasers have better thermal dissipation~~ than lasers based on SL cladding.

At 80 K, the threshold current density of this device is 18 A/cm^2 with a threshold voltage of 2.77 V, corresponding to a voltage efficiency of 96%. As shown in Fig. 3(a), as the temperature was changed, the emission wavelength (λ) was red shifted by 3.5 nm/K (from 4.67 μm at 80 K to 5.27 μm at 247 K) in cw mode. In pulsed mode, the lasing wavelength red shifted by 3.0 nm/K in the temperature range from 200 to 280 K, then red shifted at a reduced rate at higher temperatures before blue shifting slightly at the highest temperatures (Fig. 3(b)). The blue shift typically results from band filling effects that occur when the maximum operating temperature is being approached. The threshold current density of this device at 295 K in pulsed mode was 2.4 kA/cm^2.

A 30-μm-wide device (denoted as A2) lased in cw mode at temperatures up to 222 K, a lower maximum than that obtained from a 15 μm-wide device on the same bar, indicating more heating for the larger device. As shown from its current-voltage-light ($I-V-L$) characteristics (Fig. 4(a)), the cw output power of this 30-μm-wide device reached 120 mW/facet at 80 K and at 500 mA with a maximum wall-plug efficiency of ~21% at 80 K. The output power and the wall-plug efficiency mentioned above are underestimated because we only corrected for the 10% transmission loss through the cryostat's optical window and not for losses from beam divergence. Based on our simulated far-field patterns and the acceptance aperture of the power meter (diameter 19 mm) [18], the estimated additional beam divergence loss is about 30%-43% (depending on laser size). Taking this correction into account the laser's actual output power exceeded 170 mW/facet and the wall-plug efficiency was about 30% at 80 K. In pulsed operation (1 μs pulses at 1kHz), the device lased at heat-sink temperatures up to 295 K with a threshold current density around 1.3 kA/cm^2 and a threshold voltage of ~4.0 V as shown in Fig. 4(b). The differential efficiency decreased with the temperature, but more rapidly for temperatures 280 K and above, which might be indicative of increased free-carrier absorption at high temperatures.

Lasers fabricated from wafer B (hybrid dielectric-metal as the top cladding layer) showed device performance similar to (or slightly better than) lasers made from wafer A in terms of operating temperature. A 15-μm-wide and 1.25-mm-long device (device B1) lased in cw mode at temperatures up to 248 K near 5.25μm with a threshold current density of

R48

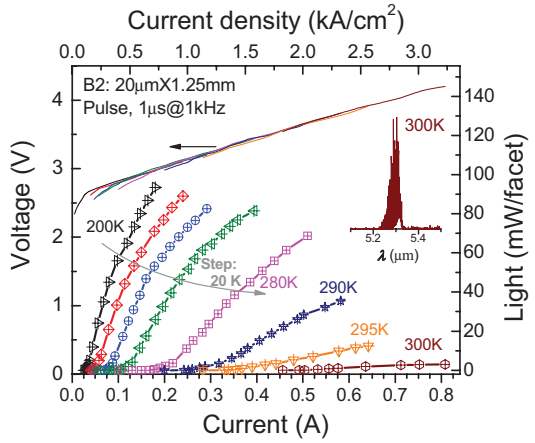

Fig. 6. Measured pulsed *I–V–L* characteristics of a 20-μm-wide and 1.25-mm-long laser (B2) from wafer B operating in pulsed mode (1-μs pulses at 1 kHz) at different heat sink temperatures. Inset is the pulsed-mode lasing spectrum at 300 K (1-μs pulses at 10 kHz).

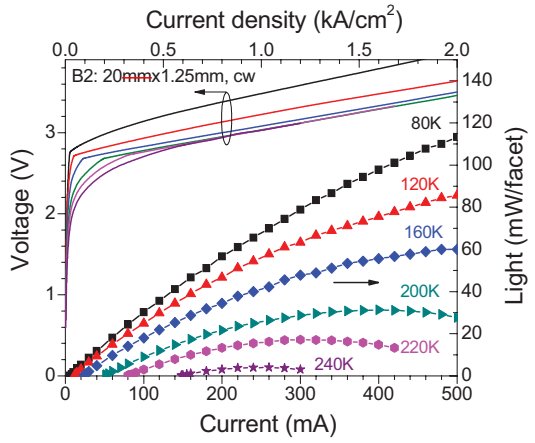

Fig. 7. Measured *I–V–L* characteristics of a 20-μm-wide and 1.25-mm-long laser (B2) from wafer B operating in cw mode at different heat sink temperatures.

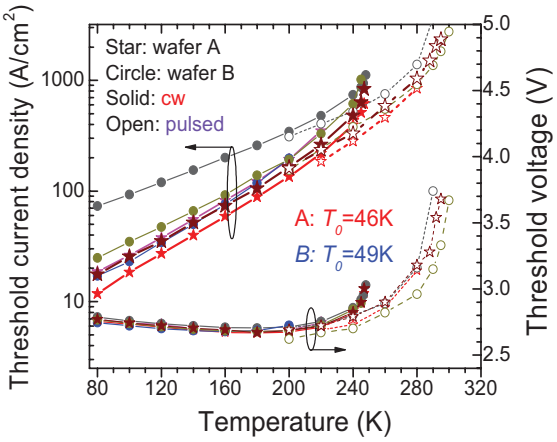

Fig. 8. Threshold current density and voltage as a function of heat sink temperature for devices made from wafers A and B in both cw and pulsed modes. The extracted characteristic temperature T_0 for the best devices from wafers A and B are 46 and 49 K, respectively.

1.1 kA/cm^2 (see Fig. 5(a)). In pulsed operation (1 μs pulse sat 10 kHz), the device lased at temperatures up to 290 K (see Fig. 5(b)), which is comparable to the maximum pulsed operating temperature (295 K) of device A1. A 20-μm-wide laser (device B2) from the same bar operated in pulsed mode at temperatures up to 300 K near 5.3 μm with a threshold current density of 2.7 kA/cm^2, as shown in the inset of Fig. 6. The maximum pulsed operating temperature (300 K) of this 20-μm-wide device is slightly higher than that of devices from wafer A. This 20-μm-wide device lased in cw mode up to 245 K with a threshold current density of 1.0 kA/cm^2. At 80 K, device B2 also delivered a cw output power of 112 mW/facet with a threshold current density of ~25 A/cm^2 and a threshold voltage of 2.77 V, as indicated by its *I-V-L* characteristics shown in Fig. 7. Again, the output power in Fig. 7 did not include the beam divergence losses.

We tested about 40 laser devices with various ridge widths and cavity lengths from wafers A and B and found that they have near identical lasing wavelengths for a wide operating temperature range (80 to 290 K) with a temperature coefficient of ~3.2 nm/K. The overall device performance is similar for lasers from wafers A and B in terms of output power, threshold current, and operating temperatures. The maximum pulsed operating temperature achieved in devices from wafer B is slightly higher than that from wafer A (300 K versus 295 K). ~~The threshold current densities of devices from wafer A were generally lower compared to devices from wafer B, particularly at low temperatures~~, as shown in Fig. 8. The lowest threshold current density of 12 A/cm^{2}at 80 K was obtained from a 15-μm-wide and 2.6-mm-long device from wafer A. One might attribute the somewhat larger threshold current densities in devices from wafer B to higher waveguide optical losses in wafer B devices compared to those from wafer A. If this were true, the maximum pulsed operating temperature achievable in devices from wafer B would be lower, which contradicts our experimental findings and modeling results. The difference in threshold current density between wafers A and B is more likely due to the higher surface-defect density of wafer B compared to wafer A, as indicated by optical microscope images. As seen in Fig. 8, the difference in threshold current density is most significant at low temperatures and becomes smaller at high temperatures. This supports the argument that material defects and processing variations are responsible for the threshold current difference because the defect-related Shockley–Read–Hall (SRH) recombination dominates at low temperatures. Similar defect effects were observed from early IC lasers [21] and type-II SL detectors, and often occur for Sb-based devices due to material nonuniformity and processing variations. Such defects probably open up additional channels for leakage current. Consequently, extra current is required to compensate for this carrier leakage channel in order to reach the lasing threshold in materials with high defect densities. These defects should *not* influence the modal gain and waveguide loss, which are the factors that ultimately determine the maximum pulsed-mode operating temperature of a laser (when heating effects can be neglected). Thus, the observed device performance is consistent with what is expected from defect-related leakage current and the

similarity in measured maximum operating temperatures, and is supported by our theoretical calculations.

To further validate our findings, two IC laser structures (wafers C and D) were grown with waveguide structures similar to wafers A and B, respectively. Wafers C and D have the same 12-stage cascade region, but they have different top cladding configurations. Wafer C has a top InAs-plasmon cladding layer and wafer D has only a thin (35 nm) n^{++}-type InAs contact layer similar to wafer B. They were processed into laser devices in the same way as wafers A and B. Our measurements indicated that devices from wafers C and D were comparable, both lased in pulsed near 5.3 μm at room temperature. The maximum pulsed operating temperature achieved for devices from wafer D (no top semiconductor-plasmon cladding layer) is 315 K, which is slightly higher than that the 310 K achieved for devices from wafer C [22]. This result supports our earlier findings.

IV. Conclusion

In summary, InAs-based interband cascade lasers at 5.3 μm with different top waveguide cladding configurations were investigated both theoretically and experimentally. In accordance with the theoretical calculations, by replacing the top InAs-plasmon waveguide cladding with a dielectric-metal hybrid cladding, the IC lasers showed comparable or slightly superior device performances. This indicates the possible absorption loss from the contact metal was reduced because we used narrow metal contacts (and IC lasers are TE polarized) so that the dielectric layer (directly on the surface of the semiconductor ridge) plays the more significant role as the top waveguide cladding layer. Thus, a top semiconductor plasmon cladding layer is not necessarily required. No such cladding layer is preferred, especially for longer wavelength IC lasers, for which a thick cladding layer and a possibly high optical loss in semiconductor waveguides becomes problematic. Other practical benefits include: (1) the MBE growth of the IC laser structure is simpler, including reduced growth time; and (2) without a top semiconductor cladding layer, a top DFB grating can be simply integrated with an IC laser for strong coupling.

The performance of the InAs-based IC lasers described above have shown significant improvement over earlier reported IC lasers with SL cladding layers and with similar low *n*-doped electron injectors operating at comparable wavelengths [19–20]. However, these lasers were not able to lase in cw operation at room temperature. Recently, the NRL group modified their cascade stage design by highly doping the InAs layers in the electron injector with Si. This was done to achieve carrier rebalancing of the internally-generated carriers and reduce the number of non-equilibrium holes at threshold. This latest innovation has pushed the cw operation of GaSb-based IC lasers above room temperature at similar wavelengths (4.7-5.6 μm) with low-power consumption [6]. Because the current InAs-based IC lasers were not designed with this carrier rebalancing, they may suffer from optical loss in the active region due to an excess hole concentration. We expect the combination of the hybrid dielectric-metal waveguide and the latest carrier rebalancing design over the cascade region will make it possible to extend room temperature, cw operation of IC lasers to longer IR wavelengths.

Acknowledgment

The authors would like to thank A. Gin and J. Nogan for their help and technical assistance. They are also grateful to K. Mansour of Jet Propulsion Laboratory, Los Angeles, CA, for device fabrication on a piece of wafer D.

References

[1] R. Q. Yang, "Infrared laser based on intersubband transitions in quantum wells," *Superlatt. Microstruct.*, vol. 17, no. 1, pp. 77–83, 1995.

[2] M. Kim, C. L. Canedy, W. W. Bewley, C. S. Kim, J. R. Linda, J. Abell, I. Vurgaftman, and J. R. Meyer, "Interband cascade laser emitting at $\lambda = 3.75$ μm in continuous wave above room temperature," *Appl. Phys. Lett.*, vol. 92, no. 19, pp. 191110-1–191110-3, 2008.

[3] W. W. Bewley, C. L. Canedy, C. S. Kim, M. Kim, J. R. Lindle, J. Abell, I. Vurgaftman, and J. R. Meyer, "Ridge-width dependence of midinfrared interband cascade laser characteristics," *Opt. Eng.*, vol. 49, p. 111116, Nov. 2010.

[4] I. Vurgaftman, W. W. Bewley, C. L. Canedy, C. S. Kim, M. Kim, J. R. Lindle, C. D. Merritt, J. Abell, and J. R. Meyer, "Mid-IR type-II interband cascade lasers," *IEEE J. Sel. Topics Quantum Electron.*, vol. 17, no. 5, pp. 1435–1444, Sep.–Oct. 2011.

[5] I. Vurgaftman, W. W. Bewley, C. L. Canedy, C. S. Kim, M. Kim, C. D. Merritt, J. Abell, J. R. Lindle, and J. R. Meyer, "Rebalancing of internally generated carriers for mid-infrared interband cascade lasers with very low power consumption," *Nature Commun.*, vol. 2, p. 585, Dec. 2011.

[6] W. W. Bewley, C. L. Canedy, C. S. Kim, M. Kim, C. D. Merritt, J. Abell, I. Vurgaftman, and J. R. Meyer, "Continuous-wave interband cascade lasers operating above room temperature at $\lambda = 4.7$–5.6 μm," *Opt. Exp.*, vol. 20, no. 3, pp. 3235–3240, 2012.

[7] K. Ohtani and H. Ohno, "An InAs-based intersubband quantum cascade laser," *Jpn. J. Appl. Phys.*, vol. 41, no. 11B, pp. L1279–1280, 2002.

[8] R. Teissier, D. Barate, A. Vicet, D. A. Yarekha, C. Alibert, A. N. Baranov, X. Marcadet, M. Garcia, and C. Sirtori, "InAs/AlSb quantum cascade lasers operating at 6.7 μm," *Electron. Lett.*, vol. 39, no. 17, pp. 1252–1254, Aug. 2003.

[9] Z. Tian, R. Q. Yang, T. D. Mishima, M. B. Santos, R. T. Hinkey, M. E. Curtis, and M. B. Johnson, "InAs-based interband cascade lasers near 6 μm," *Electron. Lett.*, vol. 45, no. 1, pp. 48–49, Jan. 2009.

[10] Z. Tian, R. Q. Yang, T. D. Mishima, M. B. Santos, and M. B. Johnson, "Plasmon-waveguide interband cascade lasers near 7.5 μm," *IEEE. Photon. Technol. Lett.*, vol. 21, no. 21, pp. 1588–1590, Nov. 2009.

[11] Z. Tian, L. Li, H. Ye, R. Q. Yang, T. D. Mishima, M. B. Santos, and M. B. Johnson, "InAs-based interband cascade lasers with emission wavelength at 10.4 μm," *Electron. Lett.*, vol. 48, no. 2, pp. 113–114, Jan. 2012.

[12] C. Sirtori, C. Gmachl, F. Capassp, J. Faist, D. Sivco, A. Hutchinson, and A. Y. Cho, "Long-wavelength ($\lambda \approx 8$–11.5 μm) semiconductor lasers with waveguides based on surface plasmons," *Opt. Lett.*, vol. 23, no. 17, pp. 1366–1368, 1998.

[13] A. D. Rakic, A. B. Djurisic, J. M. Elazar, and M. L. Majewski, "Optical properties of metallic films for vertical-cavity optoelectronic devices," *Appl. Opt.*, vol. 37, no. 22, pp. 5271–5283, 1998.

[14] Y. B. Li, R. A. Stradling, T. Knight, J. R. Birch, R. H. Thomas, C. C. Phillips, and I. T. Ferguson, "Infrared reflection and transmission of undoped and Si-doped InAs grown on GaAs by molecular beam epitaxy," *Semicond. Sci. Technol.*, vol. 8, no. 1, pp. 101–111, 1993.

[15] A. N. Baranov, private communication, 2010.

[16] A. Bauer, M. Dallner, M. Kamp, S. Hofling, L. Worschech, and A. Forchel, "Shortened injector interband cascade lasers for 3.3- to 3.6-μm emission," *Opt. Eng.*, vol. 49, p. 111117, Nov. 2010.

[17] R. Q. Yang, C. J. Hill, K. Mansour, Y. Qiu, A. Soibel, R. Muller, and P. Echternach, "Distributed feedback mid-IR interband cascade lasers at thermoelectric cooler temperatures," *IEEE J. Sel. Topics Quantum Electron.*, vol. 13, no. 5, pp. 1074–1078, Sep.–Oct. 2007.

[18] Z. Yin, Y. Jiang, Z. Tian, R. Q. Yang, T. D. Mishima, M. B. Santos, and M. B. Johnson, "Far-field patterns of plasmon waveguide interband cascade lasers," *IEEE J. Quantum Electron.*, vol. 47, no. 11, pp. 1414–1419, Nov. 2011.

[19] C. L. Canedy, W. W. Bewley, J. R. Lindle, J. A. Nolde, D. C. Larrabee, C. S. Kim, M. Kim, I. Vurgaftman, and J. R. Meyer, "Interband cascade lasers with wavelengths spanning 2.9 μm to 5.2 μm," *J. Electron. Mater.*, vol. 37, no. 12, pp. 1780–1785, 2008.
[20] C. J. Hill and R. Q. Yang, "MBE growth optimization of Sb-based interband cascade lasers," *J. Cryst. Growth*, vol. 278, nos. 1–4, pp. 167–172, 2005.
[21] R. Q. Yang, J. D. Bruno, J. L. Bradshaw, J. T. Pham, and D. E. Wortman, "Interband cascade lasers: Progress and challenges," *Phys. E*, vol. 7, nos. 1–2, pp. 69–75, 2000.
[22] Y. Jiang, L. Li, Z. Tian, R. T. Hinkey, R. Q. Yang, T. D. Mishima, M. B. Santos, M. B. Johnson, and K. Mansour, "Room-temperature InAs-based interband cascade lasers," in *Proc. 14th Conf. Lasers Electro-Opt.*, 2012, paper CF3K.1.

Zhaobing Tian (M'12) received the B.E. degree in electrical engineering from Xi'an Jiaotong University, Xi'an, China, and the Ph.D. degree in solid-state and microelectronics from the Shanghai Institute of Microsystem and Information Technology, Chinese Academy of Sciences, Shanghai, China, in 2003 and 2008, respectively.

He was with the School of Electrical and Computer Engineering, University of Oklahoma, Norman from May 2008 to March 2012. He is currently with the Center for High Tech Materials, University of New Mexico. His research interests include physics and development of infrared optoelectronic devices, including lasers, detectors, and photovoltaic devices.

Yuchao Jiang received the B.S. degree from the Beijing University of Posts and Telecommunications, Beijing, China, and the M.S. degree from the Institute of Semiconductors, Chinese Academy of Science, Beijing, China, in 2007 and 2011, respectively. He is currently pursuing the Ph.D. degree from the University of Oklahoma, Norman.

His current research interests include modeling and characterization of mid-infrared optoelectronic devices, including quantum and interband cascade lasers.

Lu Li received the B.S. degree in physics from Central China Normal University, Wuhan, China, and the Ph.D. degree in material physics and chemistry from the Institute of Semiconductors, Chinese Academy of Sciences, Beijing, China, in 2001 and 2008, respectively.

He has been an Assistant Research Fellow with the Key Laboratory of Semiconductor Materials, Chinese Academy of Sciences, since 2008. He is currently working with Dr. Yang's and Dr. Santo's groups as a Post-Doctoral Researcher at the University of Oklahoma, Norman. His current research interests include molecular beam epitaxy growth of infrared optoelectronic devices, including quantum and interband cascade lasers and detectors.

Robert T. Hinkey was born in Baltimore, MD, in 1985. He received the B.S. degree in physics from Loyola University, Baltimore, in 2007, and the M.S. degree in engineering physics from the University of Oklahoma, Norman, in 2011. He is currently pursuing the Ph.D. degree with the University of Oklahoma.

His current research interests include waveguides for interband cascade lasers and the transport properties of interband cascade infrared photodetectors and photovoltaic devices.

Zuowei Yin was born in Yancheng, China, in 1985. He received the B.S. degree from Nanjing University, Nanjing, China, in 2007. He is currently pursuing the Ph.D. degree with the National Laboratory of Microstructures, School of Engineering and Applied Sciences, Nanjing University.

He was supported by China Council Scholarship as a Visiting Graduate Student from 2010 to 2011 with the University of Oklahoma, Norman. His current research interests include fiber communication and semiconductor devices such as interband cascade lasers.

Rui Q. Yang (M'95–SM'02) received the Ph.D. degree in physics from Nanjing University, Nanjing, China, in 1987.

He is a Professor with the School of Electrical and Computer Engineering, University of Oklahoma (OU), Norman, with research activities ranging from condensed matter physics to semiconductor quantum devices such as mid-infrared lasers, detectors, and photovoltaic devices. Prior to joining OU, in 2007, he was a Principal Engineering Staff Member and a Task Manager with Jet Propulsion Laboratory (JPL), Pasadena, CA. He has authored or co-authored more than 100 refereed journal articles and one book chapter.

Dr. Yang received the Edward Stone Award from JPL for Outstanding Research Publication in 2007 and the successful accelerated infusion of cutting-edge interband cascade semiconductor laser technology into flight mission readiness.

Tetsuya D. Mishima received the Ph.D. degree from Waseda University, Tokyo, Japan, in 1999.

He has been a Research Scientist with the University of Oklahoma, Norman, since 2001. He previously held a post-doctoral position with Pennsylvania State University, University Park, from 1999 to 2001. He is the co-author of over 70 scientific publications. His current research interests include structural defect reduction in semiconductor structures grown by molecular beam epitaxy, development of transmission electron microscopy techniques for structural defect analysis, and theoretical analysis on carrier transport in quantum well structures.

Michael B. Santos received the B.S. degree in electrical engineering and materials science from Cornell University, Ithaca, NY, and the Ph.D. degree in electrical engineering from Princeton University, Princeton, NJ, in 1986 and 1992, respectively.

He was a Post-Doctoral Researcher with AT&T Bell Laboratories, Holmdel, NJ, before joining the University of Oklahoma, Norman, in 1993. He is currently a Professor of physics with the University of Oklahoma. He has co-authored 190 papers on experimental semiconductor research.

Matthew B. Johnson received the B.S. degree in physics from the University of Waterloo, Waterloo, ON, Canada, and the Ph.D. degree in applied physics from the California Institute of Technology, Pasadena, in 1979 and 1989, respectively.

He has been a Physics Faculty Member with the University of Oklahoma, Norman, since 1995. He previously held post-doctoral positions with IBM Research, Yorktown Heights, NY, and IBM Research, Zürich, Switzerland. He has been serving as the Director of the Center for Semiconductor Physics in Nanostructures, National Science Foundation Materials Research Science and Engineering Center with members at the University of Oklahoma, and the University of Arkansas, Fayetteville, since 2000. He has co-authored over 100 scientific publications.